

## Electronic Supplementary Information

### Efficient Photorelease of Carbon Monoxide from a Luminescent Tricarbonyl Rhenium(I) Complex Incorporating Pyridyl-1,2,4-triazole and Phosphine Ligands

Ángel Hernández Mejías, Alexandre Poirot, Meriem Rmili, Nadine Leygue, Mariusz Wolff, Nathalie Saffon-Merceron, Eric Benoist and Suzanne Fery-Forgues \*

#### NMR characterization

<b>Figure S1.</b> $^1\text{H}$ NMR spectrum of $[\text{Re}(\text{CO})_3(\text{L})(\text{CH}_3\text{CN})]^+(\text{OTf})^-$ in $\text{CD}_3\text{CN}$ .....	2
<b>Figure S2.</b> $^{13}\text{C}$ NMR spectrum of $[\text{Re}(\text{CO})_3(\text{L})(\text{CH}_3\text{CN})]^+(\text{OTf})^-$ in $\text{CD}_3\text{CN}$ .....	2
<b>Figure S3.</b> COSY NMR spectrum of $[\text{Re}(\text{CO})_3(\text{L})(\text{CH}_3\text{CN})]^+(\text{OTf})^-$ in $\text{CD}_3\text{CN}$ .....	3
<b>Figure S4.</b> HSQC NMR spectrum of $[\text{Re}(\text{CO})_3(\text{L})(\text{CH}_3\text{CN})]^+(\text{OTf})^-$ in $\text{CD}_3\text{CN}$ .....	3
<b>Figure S5.</b> HMBC NMR spectrum of $[\text{Re}(\text{CO})_3(\text{L})(\text{CH}_3\text{CN})]^+(\text{OTf})^-$ in $\text{CD}_3\text{CN}$ .....	4
<b>Figure S6.</b> Numbering scheme and $^1\text{H}$ NMR spectrum of <b>1-TPP</b> in $\text{CD}_3\text{CN}$ .....	4
<b>Figure S7.</b> $^{13}\text{C}$ NMR spectrum of <b>1-TPP</b> in $\text{CD}_3\text{CN}$ .....	5
<b>Figure S8.</b> COSY NMR spectrum of <b>1-TPP</b> in $\text{CD}_3\text{CN}$ .....	5
<b>Figure S9.</b> HSQC NMR spectrum of <b>1-TPP</b> in $\text{CD}_3\text{CN}$ .....	6
<b>Figure S10.</b> HMBC NMR spectrum of <b>1-TPP</b> in $\text{CD}_3\text{CN}$ .....	6

#### Molecular structure

<b>Figure S11.</b> Molecular view showing the stacking of PBO moieties in molecules of <b>1-TPP</b> .....	7
<b>Table S1.</b> Experimental and theoretical selected bond lengths and angles for complex <b>1-TPP</b> in $\text{CH}_3\text{CN}$ .....	7

#### Spectroscopy

<b>Figure S12.</b> Monitoring by UV-vis absorption spectroscopy of the chemical stability of <b>1-TPP</b> in $\text{CH}_3\text{CN}$ .....	7
<b>Table S2.</b> UV-vis absorption and emission properties of complex <b>1-TPP</b> in three organic solvents .....	8

#### Photochemistry

<b>Figure S13.</b> Monitoring by UV-vis absorption spectroscopy of the photochemical reaction of <b>1-TPP</b> in acetonitrile solution under irradiation at 300 nm over 12 min .....	8
<b>Figure S14.</b> Monitoring by UV-vis absorption spectroscopy of the photochemical reaction of <b>1-Cl</b> in $\text{CH}_3\text{CN}$ upon irradiation at 300 nm over 2 h .....	8
<b>Figure S15.</b> Photoluminescence spectrum of complex <b>2</b> , obtained after complete photolysis of <b>1-TPP</b> in acetonitrile solution ( $4.4 \times 10^{-5}$ M) with irradiation at 350 nm.....	9
<b>Figure S16.</b> Optical microscopy image of the microcrystalline powder of <b>1-TPP</b> suspended in water, after 10 min illumination by the microscope light beam (450 nm) .....	9
<b>Figure S17.</b> Enlargement of the $^1\text{H}$ NMR spectrum of <b>1-TPP</b> in $\text{CD}_3\text{CN}$ .....	9
<b>Figure S18.</b> High resolution mass spectrum ESI $^+$ and chemical structure of complex <b>2</b> .....	10

#### DFT and TD-DFT calculations

<b>Table S3.</b> Frontier molecular orbital compositions (%) and energy levels in $\text{CH}_3\text{CN}$ for <b>1-TPP</b> .....	10
<b>Table S4.</b> Main electronic transitions for <b>1-TPP</b> in $\text{CH}_3\text{CN}$ , calculated with TD-DFT method .....	11
<b>Table S5.</b> Four calculated singlet states for <b>1-TPP</b> in $S_1$ optimized geometry with TD-DFT method .....	11
<b>Table S6.</b> Calculated phosphorescence emission energies of <b>1-TPP</b> in acetonitrile .....	11
<b>Figure S19.</b> Isodensity plots of the frontier molecular orbitals of <b>1-TPP</b> in $\text{CH}_3\text{CN}$ .....	12
<b>Figure S20.</b> Experimental and simulated UV-Vis absorption spectra of <b>1-TPP</b> and <b>2</b> in $\text{CH}_3\text{CN}$ .....	13
<b>Figure S21.</b> Spin density distribution for the lowest triplet state $T_1$ of <b>1-TPP</b> and <b>2(iso1)</b> in $\text{CH}_3\text{CN}$ .....	13
<b>Figure S22.</b> Optimized geometries of isomers 1-5 of $[\text{Re}(\text{CO})_2(\text{L})(\text{PPh}_3)(\text{CH}_3\text{CN})]^+$ (the cation of <b>2</b> ) .....	13
<b>Table S7.</b> Theoretical selected bond lengths and angles for <b>2(iso1)</b> in $\text{CH}_3\text{CN}$ .....	14
<b>Table S8.</b> Frontier molecular orbital compositions (%) and energy levels in $\text{CH}_3\text{CN}$ for <b>2(iso1)</b> .....	14
<b>Table S9.</b> Main electronic transitions for <b>2(iso1)</b> in $\text{CH}_3\text{CN}$ , calculated with TDDFT method .....	15
<b>Table S10.</b> Four calculated singlet states for <b>2(iso1)</b> in $S_1$ optimized geometry with TDDFT method .....	15
<b>Table S11.</b> Calculated phosphorescence emission energies of <b>2(iso1)</b> in acetonitrile .....	15
<b>Figure S23.</b> Isodensity plots of the frontier molecular orbitals of <b>2(iso1)</b> in $\text{CH}_3\text{CN}$ .....	16
<b>Figure S24.</b> Comparative energy levels of selected frontier molecular orbitals of <b>1-TPP</b> and <b>2(iso1)</b> in acetonitrile, and <b>1-Cl</b> in $\text{CH}_2\text{Cl}_2$ according to TD-DFT calculations .....	17

### NMR characterization

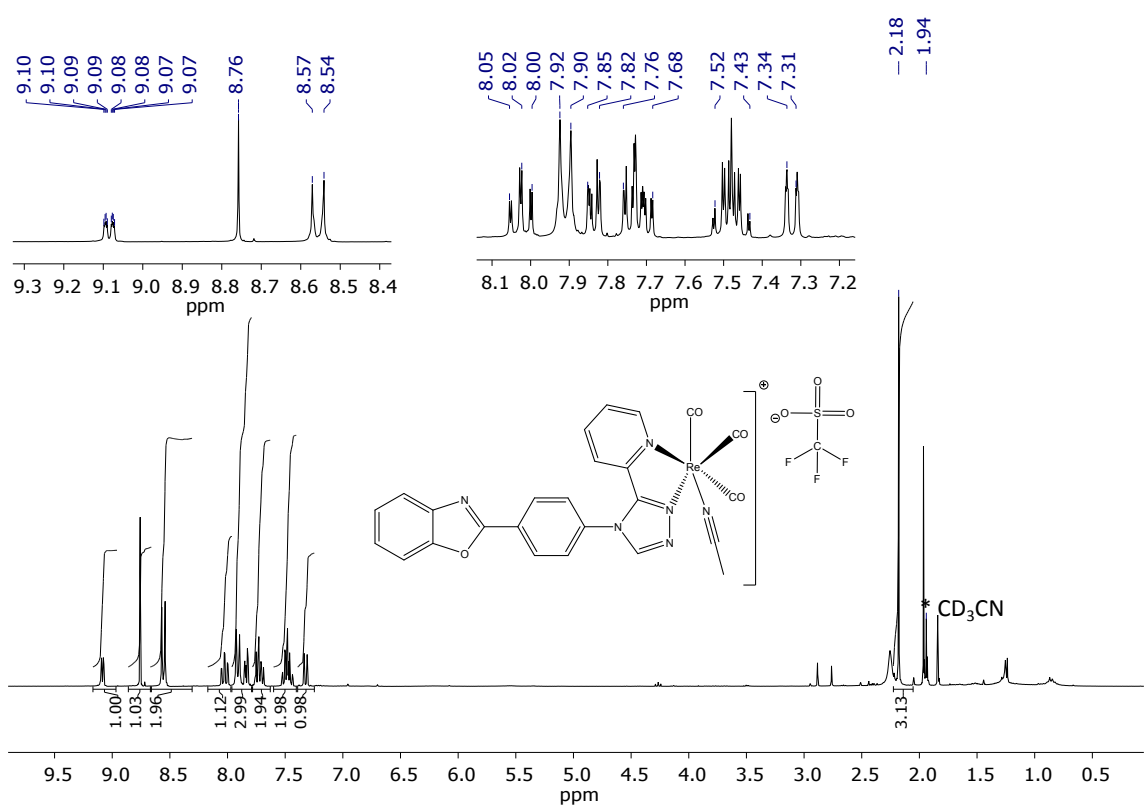


**Figure S1.**  $^1\text{H}$  NMR spectrum of  $[\text{Re}(\text{CO})_3(\text{L})(\text{CH}_3\text{CN})]^+(\text{OTf})^-$  in  $\text{CD}_3\text{CN}$ .

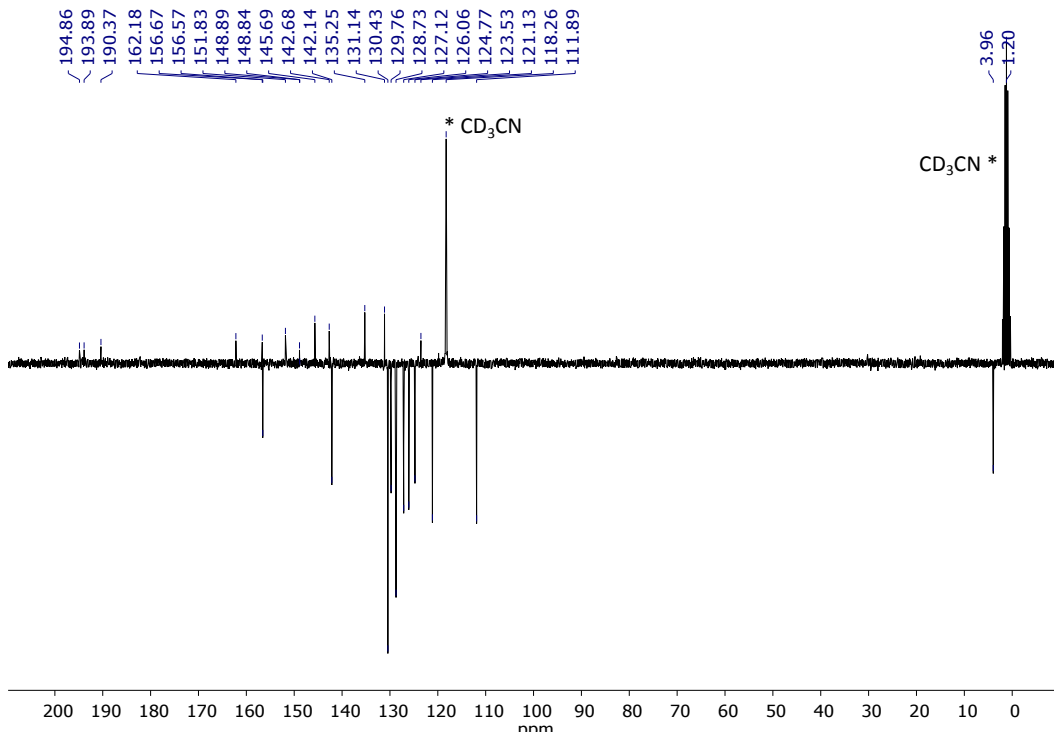


**Figure S2.**  $^{13}\text{C}$  NMR spectrum of  $[\text{Re}(\text{CO})_3(\text{L})(\text{CH}_3\text{CN})]^+(\text{OTf})^-$  in  $\text{CD}_3\text{CN}$ .

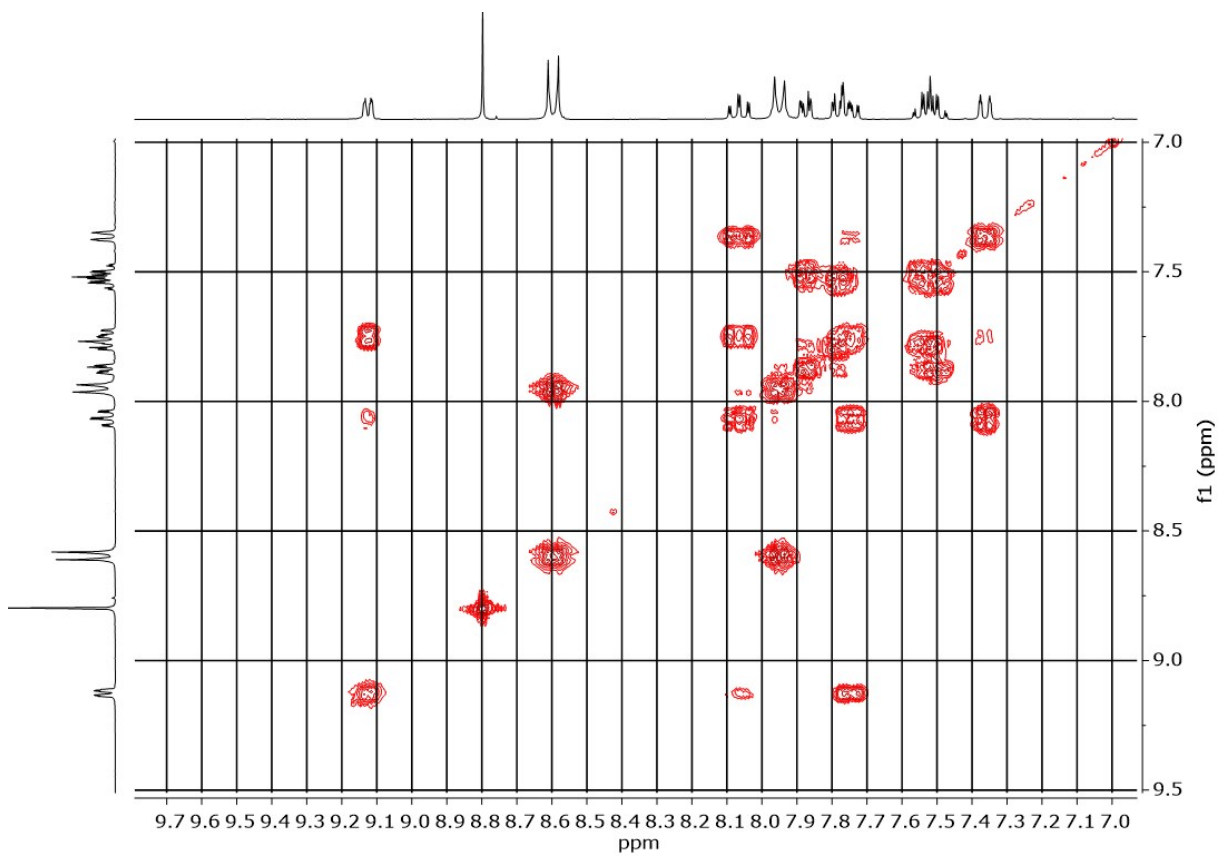


**Figure S3.** COSY NMR spectrum of  $[\text{Re}(\text{CO})_3(\text{L})(\text{CH}_3\text{CN})]^+(\text{OTf})^-$  in  $\text{CD}_3\text{CN}$ .

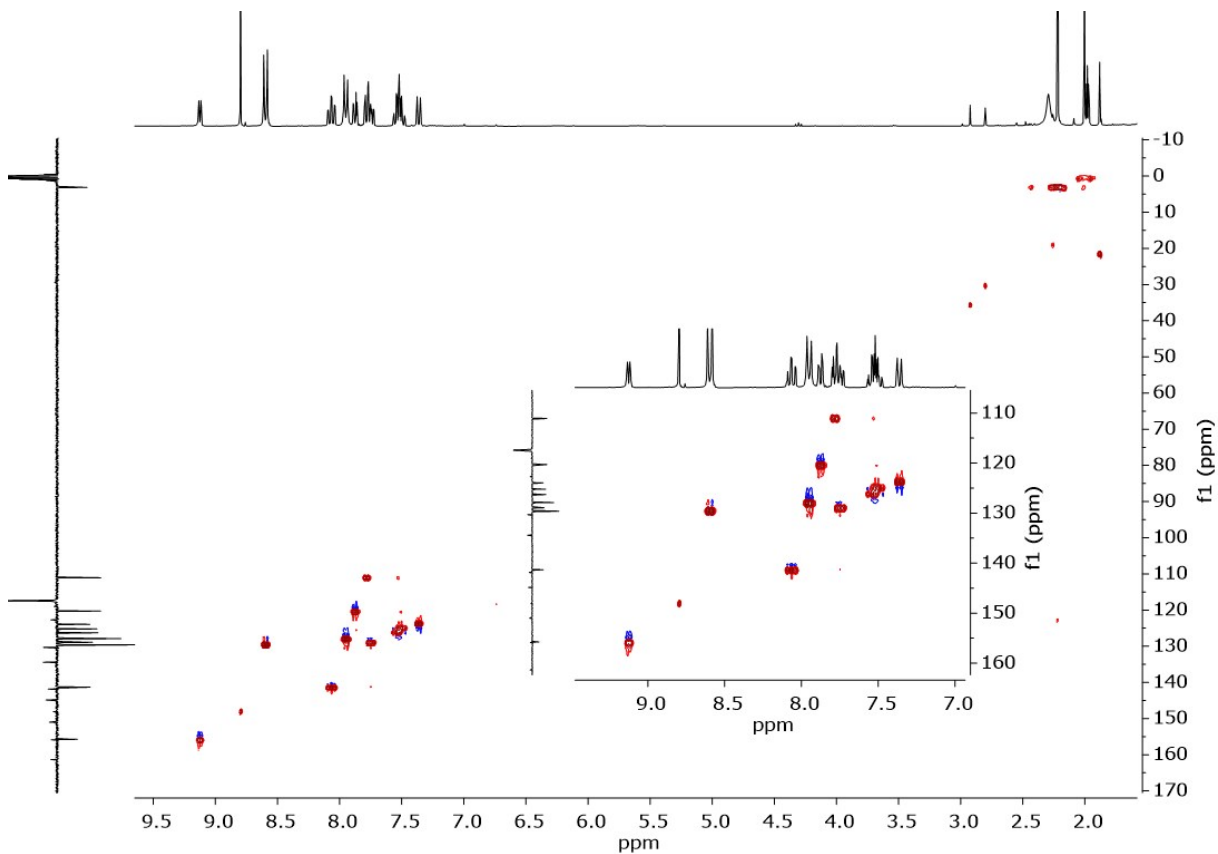


**Figure S4.** HSQC NMR spectrum of  $[\text{Re}(\text{CO})_3(\text{L})(\text{CH}_3\text{CN})]^+(\text{OTf})^-$  in  $\text{CD}_3\text{CN}$ .

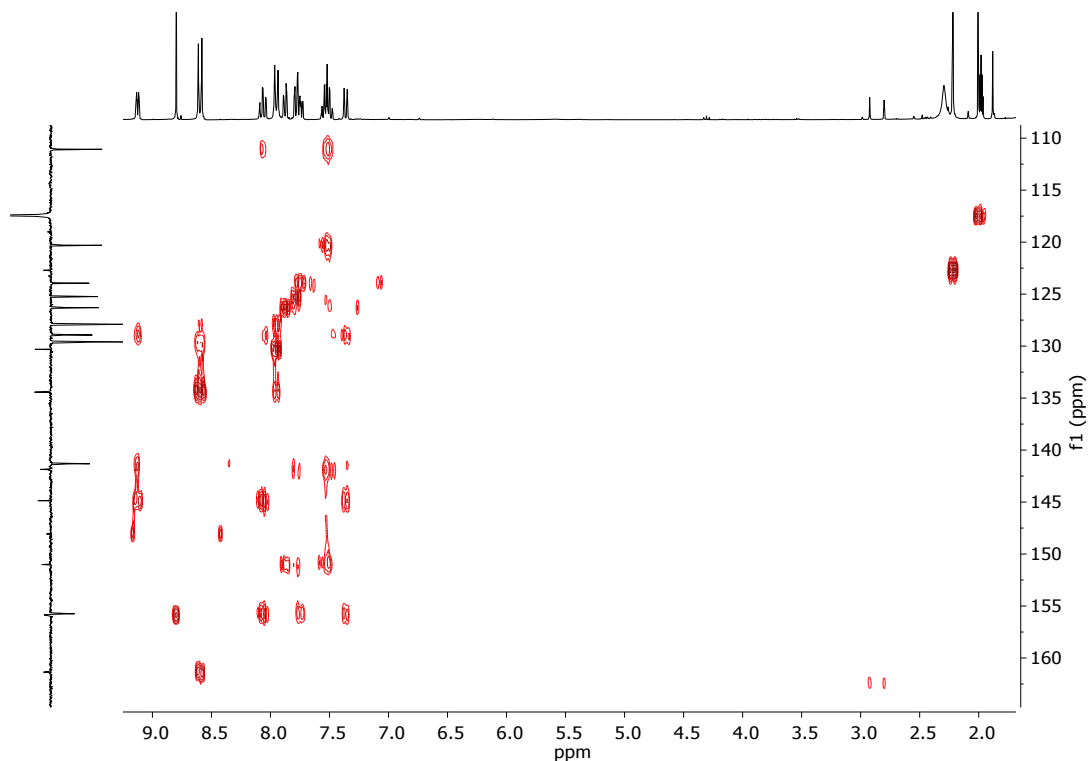


**Figure S5.** HMBC NMR spectrum of  $[\text{Re}(\text{CO})_3(\text{L})(\text{CH}_3\text{CN})]^+(\text{OTf})^-$  in  $\text{CD}_3\text{CN}$ .

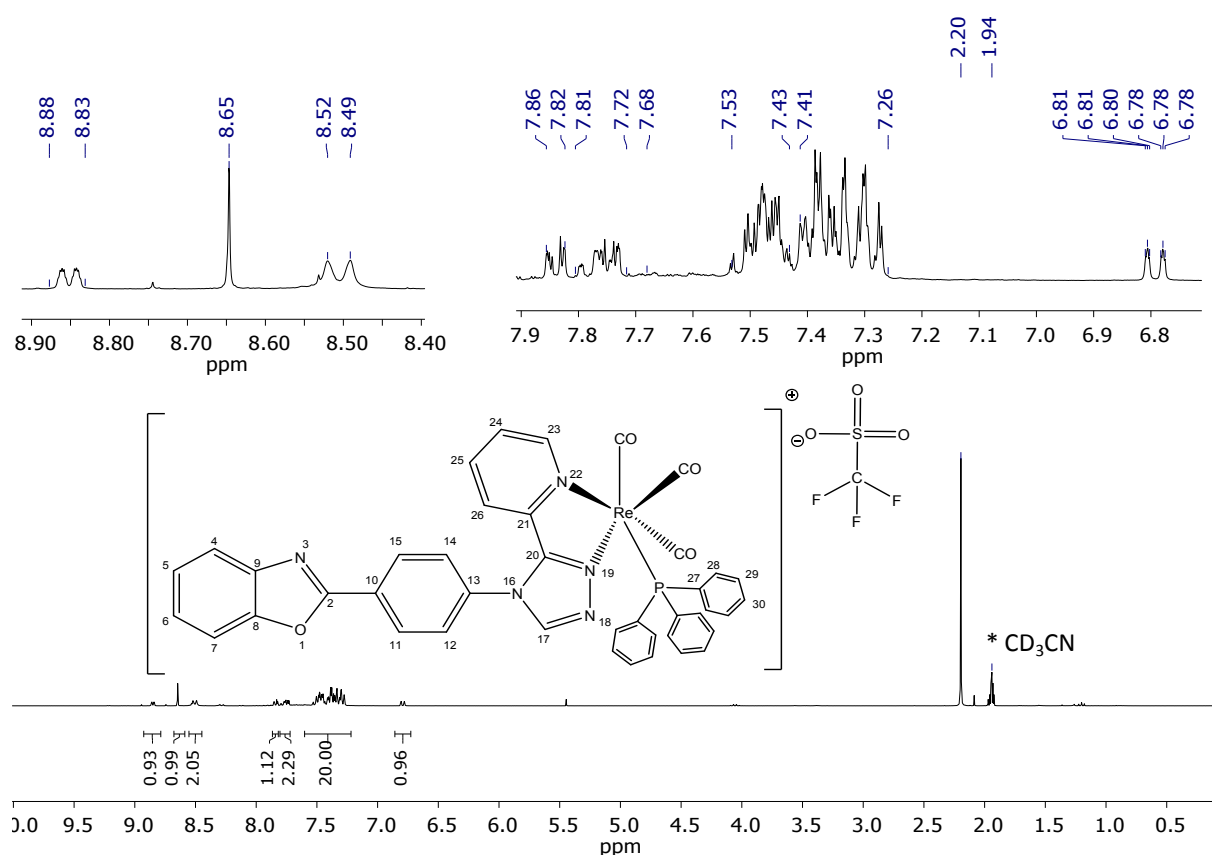


**Figure S6.** Numbering scheme and  $^1\text{H}$  NMR spectrum of  $[\text{Re}(\text{CO})_3(\text{L})(\text{PPh}_3)]^+(\text{OTf})^-$  (**1-TPP**) in  $\text{CD}_3\text{CN}$ .

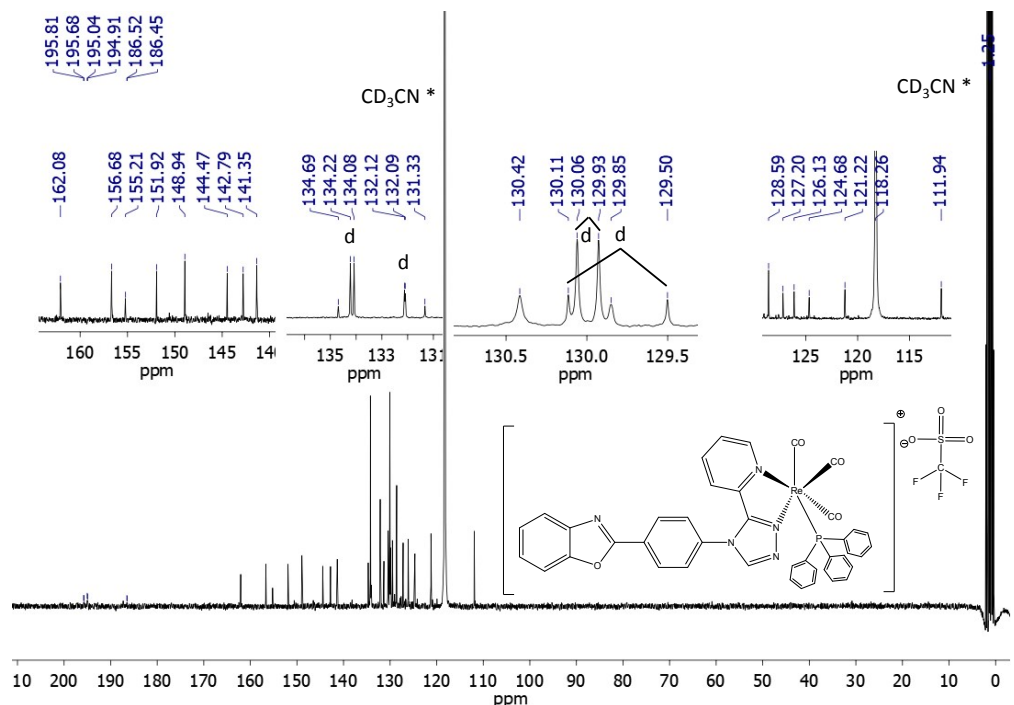


**Figure S7.**  $^{13}\text{C}$  NMR spectrum of  $[\text{Re}(\text{CO})_3(\text{L})(\text{PPh}_3)]^+(\text{OTf})^-$  (**1-TPP**) in  $\text{CD}_3\text{CN}$ .

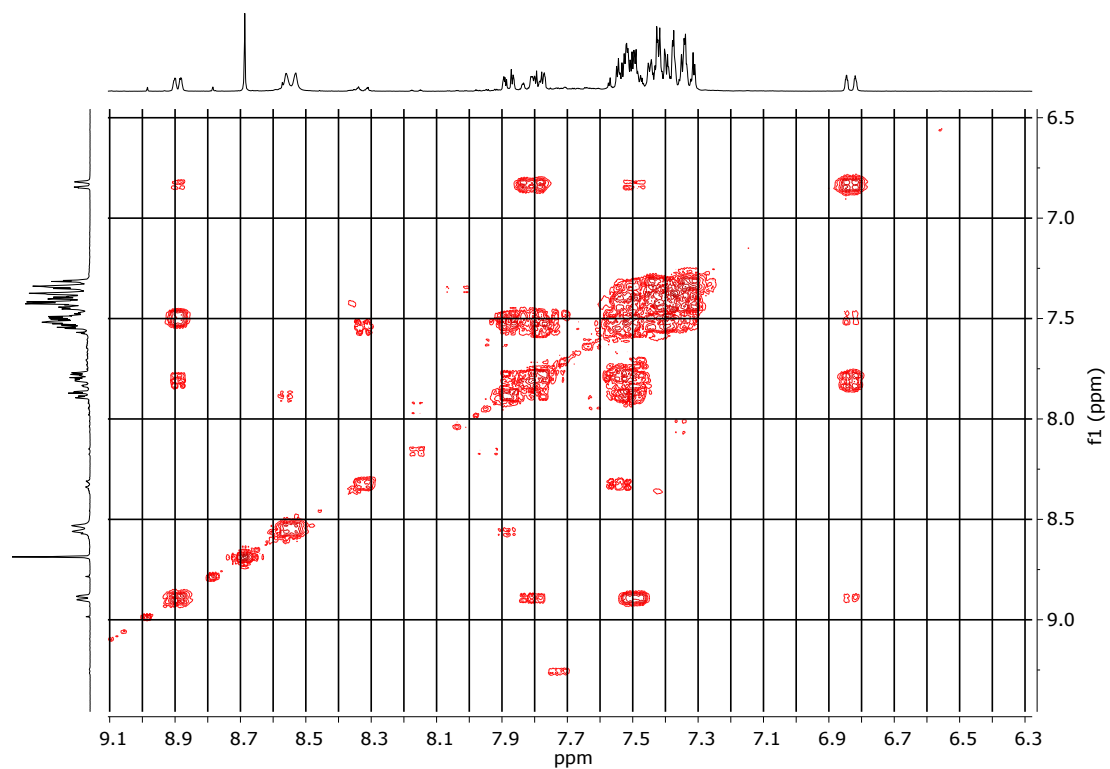


**Figure S8.** COSY NMR spectrum of  $[\text{Re}(\text{CO})_3(\text{L})(\text{PPh}_3)]^+(\text{OTf})^-$  (**1-TPP**) in  $\text{CD}_3\text{CN}$ .

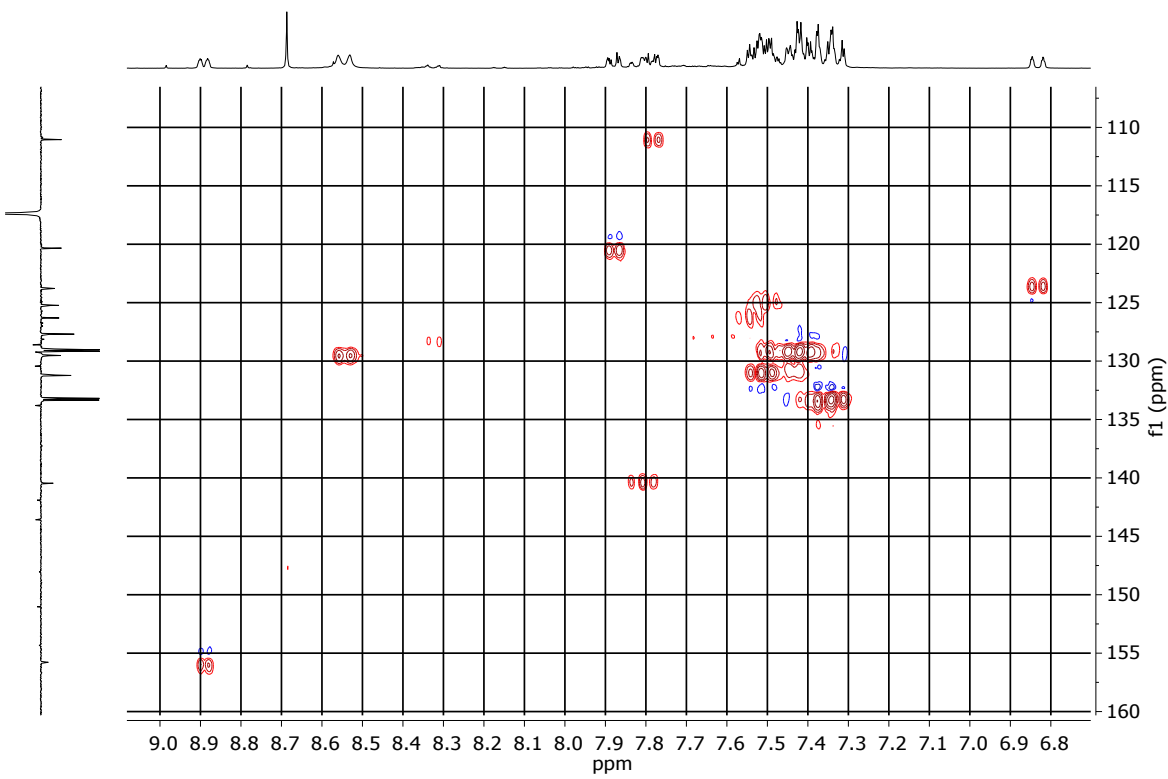


**Figure S9.** HSQC NMR spectrum of  $[\text{Re}(\text{CO})_3(\text{L})(\text{PPh}_3)]^+(\text{OTf})^-$  (**1-TPP**) in  $\text{CD}_3\text{CN}$ .

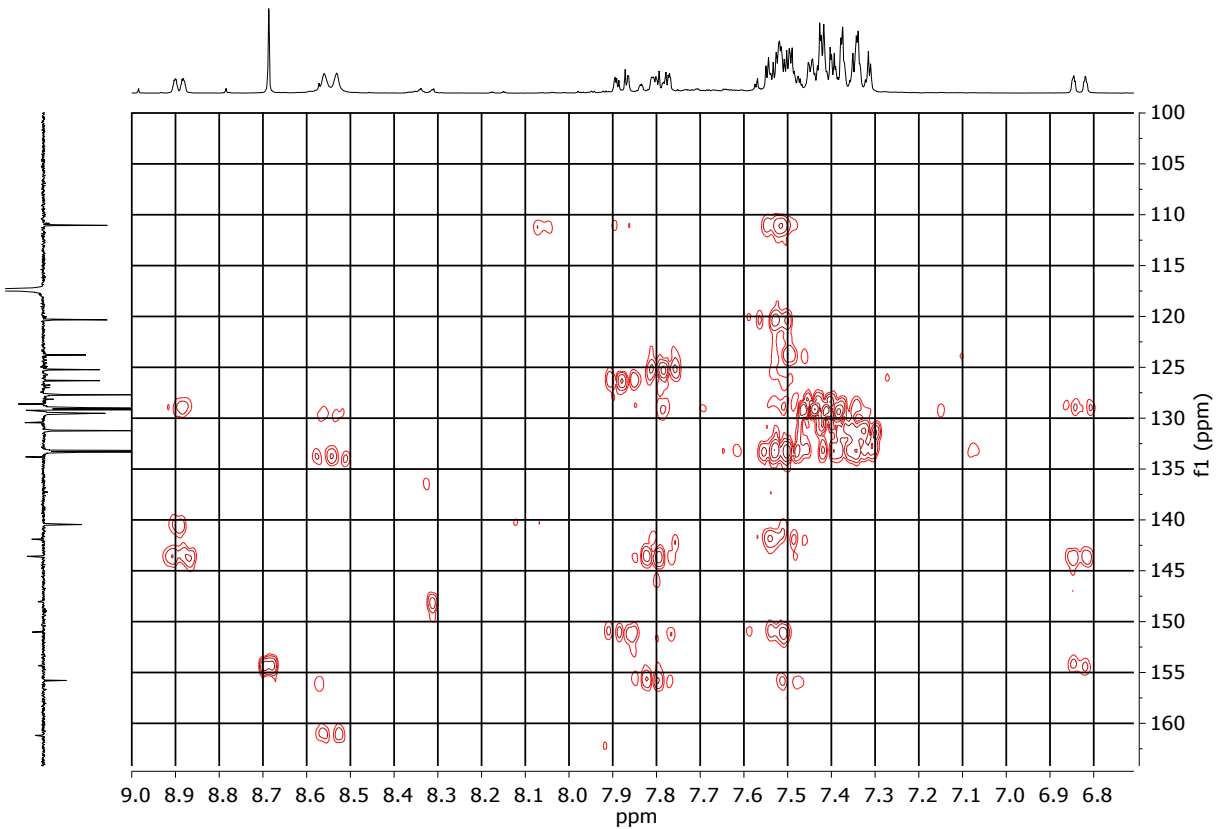


**Figure S10.** HMBC NMR spectrum of  $[\text{Re}(\text{CO})_3(\text{L})(\text{PPh}_3)]^+(\text{OTf})^-$  (**1-TPP**) in  $\text{CD}_3\text{CN}$ .

### Molecular structure

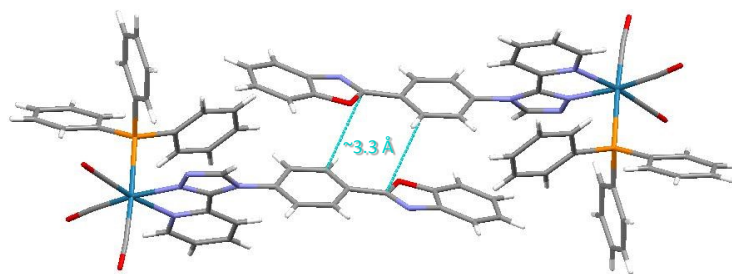


**Figure S11.** Molecular view showing the stacking of PBO moieties in molecules of **1-TPP**. Triflate and solvent molecule have been deleted for the sake of clarity.

**Table S1.** Experimental (XR data) and theoretical selected bond lengths [ $\text{\AA}$ ] and angles [ $^\circ$ ] calculated for complex **1-TPP** in  $\text{CH}_3\text{CN}$ .

Bond lengths	Exp.	Optimized			Bond angles	Exp.	Optimized		
		$S_0$	$S_1$	$T_1$			$S_0$	$S_1$	$T_1$
Re(1)-C(39)	1.900(7)	1.917	1.950	1.918	C(39)-Re(1)-C(40)	91.6(2)	90.38	85.37	90.46
Re(1)-C(40)	1.900(6)	1.918	1.969	1.918	C(39)-Re(1)-C(41)	87.7(3)	89.29	94.52	89.33
Re(1)-C(41)	1.956(7)	1.941	1.999	1.941	C(40)-Re(1)-C(41)	87.5(2)	89.03	87.10	88.97
Re(1)-N(2)	2.136(4)	2.158	2.078	2.155	C(39)-Re(1)-N(2)	97.2(2)	99.60	99.03	99.49
Re(1)-N(1)	2.196(4)	2.214	2.147	2.212	C(40)-Re(1)-N(2)	171.1(2)	170.01	175.18	170.04
Re(1)-P(1)	2.495 (2)	2.536	2.564	2.536	C(41)-Re(1)-N(2)	91.6(2)	90.77	90.58	90.78
					C(39)-Re(1)-N(1)	170.4(2)	173.14	175.47	172.99
O(2)-C(39)	1.159(7)	1.158	1.150	1.158	C(40)-Re(1)-N(1)	97.9(2)	96.41	99.12	96.45
O(3)-C(40)	1.168(6)	1.158	1.148	1.159	C(41)-Re(1)-N(1)	93.7(2)	89.83	85.09	89.65
O(4)-C(41)	1.145(7)	1.153	1.141	1.154	N(2)-Re(1)-N(1)	73.3(2)	73.61	76.46	73.59
					C(39)-Re(1)-P(1)	89.7(2)	89.98	90.94	89.93
					C(40)-Re(1)-P(1)	90.7(2)	91.81	93.40	91.79
					C(41)-Re(1)-P(1)	176.7 (2)	178.89	174.55	178.94
					N(2)-Re(1)-P(1)	90.6 (1)	88.53	88.52	88.60
					N(1)-Re(1)-P(1)	89.2 (1)	90.80	89.47	90.99
					O(2)-C(39)-Re(1)	177.2(5)	178.60	178.27	178.63
					O(3)-C(40)-Re(1)	175.8(5)	177.42	177.18	177.34
					O(4)-C(41)-Re(1)	173.6(6)	178.01	179.01	178.02

### Spectroscopy

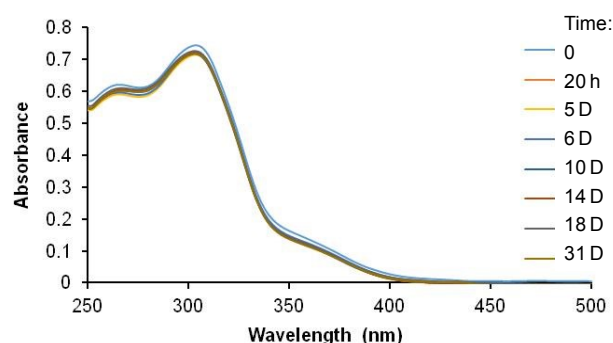


**Figure S12.** Monitoring by UV-vis absorption spectroscopy of the stability of complex **1-TPP** in  $\text{CH}_3\text{CN}$  ( $2.43 \times 10^{-5} \text{ M}$ ) in the dark over one month. The small variation between the two first measurements can be attributed to slow equilibration.

**Table S2.** UV-vis absorption and emission properties of complex **1-TPP** in three organic solvents. Excitation near the absorption maximum.

Solvent	$\lambda_{\text{abs}}$ (nm)	$\lambda_{\text{em}}$ (nm)	$\Phi_p$
Dichloromethane	306	548	0.090
Acetonitrile	305	546	0.033
Methanol	306	550	0.025

### Photochemistry

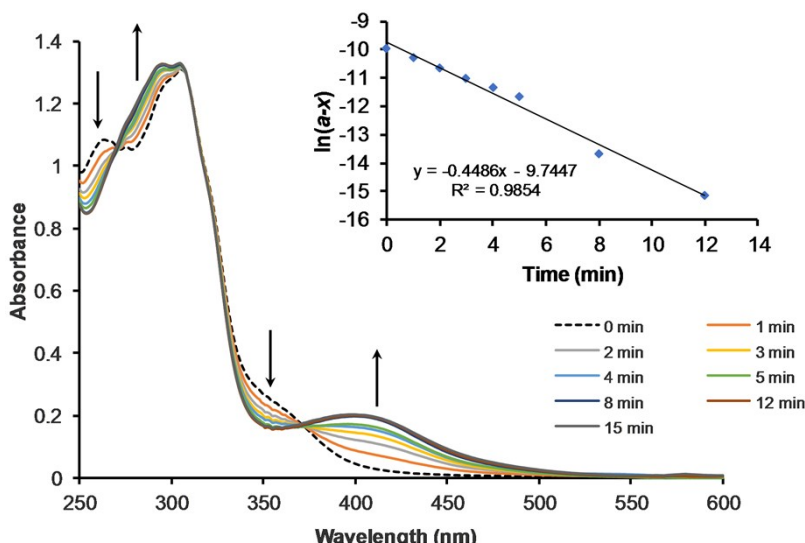


**Figure S13.** Monitoring by UV-vis absorption spectroscopy of the photochemical reaction of complex **1-TPP** in  $\text{CH}_3\text{CN}$  solution ( $4.27 \times 10^{-5}$  M) under irradiation at 300 nm over 12 min. Initial spectrum in black dashed line. The arrows indicate the evolution of the spectrum. Inset: plot of  $\log(a-x)$  vs time, with  $a$  being the initial concentration of **1-TPP** and  $x$  the concentration of formed photoproduct. According to Beer-lambert's law,  $(a-x)$  was calculated using the formula:  $a-x = a[1-(A_t-A_0)/(A_F-A_0)]$  with  $A$ : absorbance at 410 nm before reaction ( $A_0$ ), at time  $t$  ( $A_t$ ) and at  $t = 12$  min ( $A_F$ ).

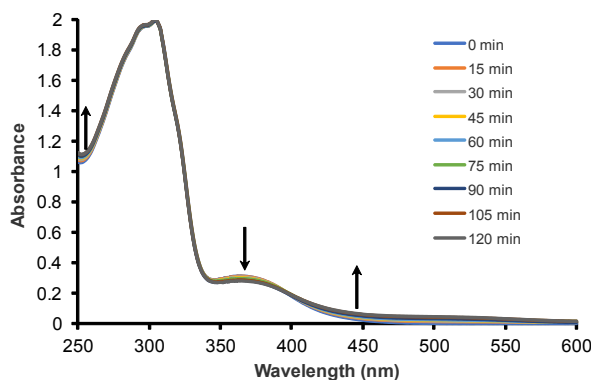


**Figure S14.** Monitoring by UV-vis absorption spectroscopy of the photochemical reaction of complex **1-Cl** in  $\text{CH}_3\text{CN}$  ( $6.4 \times 10^{-5}$  M) upon irradiation at 300 nm over 2 h. One measurement every 15 min. The arrows indicate the evolution of the spectrum.

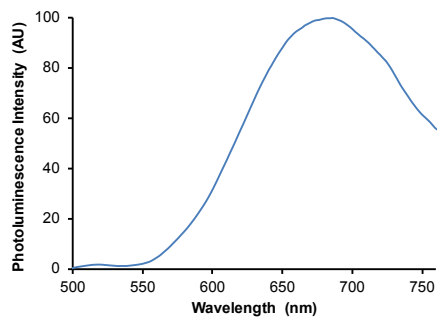


**Figure S15.** Photoluminescence spectrum of complex **2**, obtained after complete photolysis of complex **1-TPP** in CH<sub>3</sub>CN solution ( $2.1 \times 10^{-5}$  M) with irradiation at 350 nm.  $\lambda_{\text{ex}} = 370$  nm.

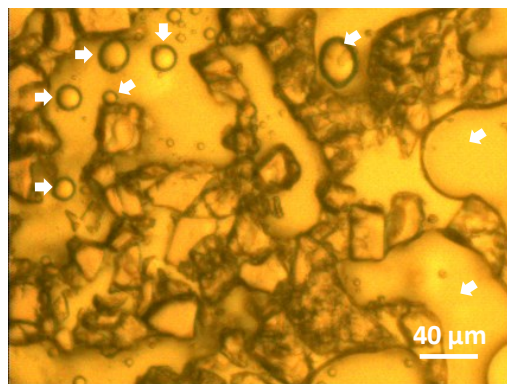


**Figure S16.** Optical microscopy image of the microcrystalline powder of complex **1-TPP** suspended in water, after 10 min illumination by the microscope light beam (450 nm). Gas bubbles are indicated by arrows.

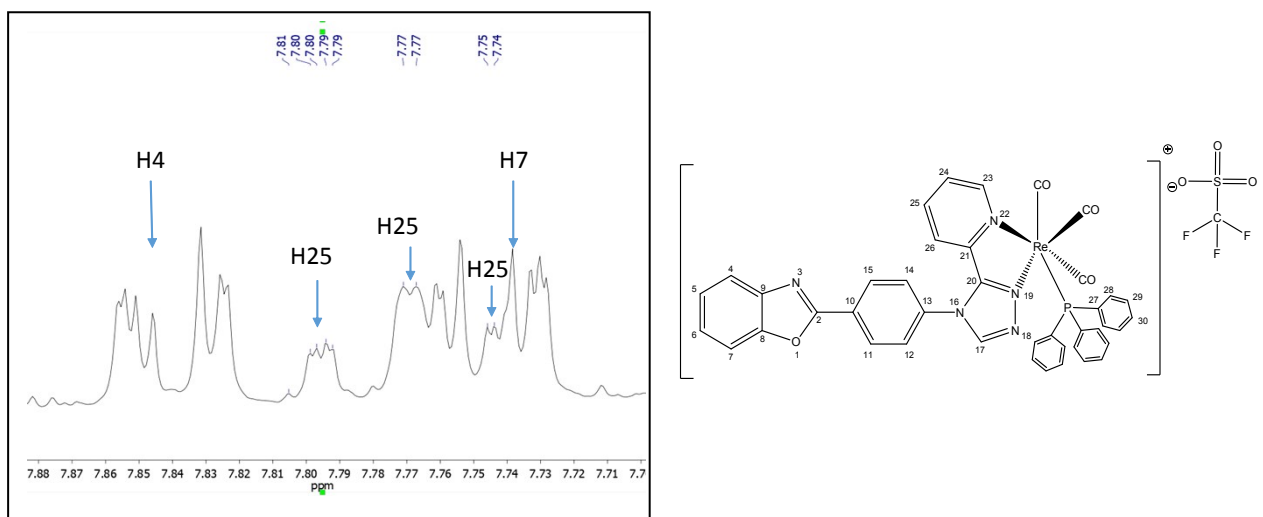


**Figure S17.** Enlargement of the <sup>1</sup>H NMR spectrum of complex **1-TPP** in CD<sub>3</sub>CN. Proton H25 appears as a very complicated apparent triplet system, the most deshielded part of which is situated between two other multiplets (H4 at the left side, and H7 at the right side, together with the rest of the signal of H25). This spectrum corresponds to t = 0 in Fig. 6. At t = 19 min in Fig. 6, the whole triplet of H25 is well visible at the right of H7.

Mass	Calc. Mass	mDa	PPM	DBE	i-FIT	Norm	Conf (%)	Formula
383.1729	883.1730	-0.1	-0.1	50.5	299.3	2.547	7.83	C58 H23 N6 O5
	883.1733	-0.4	-0.5	46.0	299.4	2.573	7.63	C54 H26 N7 O5 P
	883.1725	0.4	0.5	31.0	299.1	2.325	9.77	C42 H31 N6 O3 P 185Re
	883.1735	-0.6	-0.7	35.0	299.9	3.059	4.69	C48 H30 N2 O4 185Re
	883.1722	0.7	0.8	35.5	299.3	2.461	8.53	C46 H28 N5 O3 185Re
	883.1720	0.9	1.0	46.5	298.8	2.034	13.08	C52 H24 N10 O4 P
	883.1738	-0.9	-1.0	30.5	300.0	3.196	4.09	C44 H33 N3 O4 P 185Re
	883.1717	1.2	1.4	51.0	298.9	2.136	11.81	C56 H21 N9 O4
	883.1743	-1.4	-1.6	55.5	299.9	3.066	4.66	C59 H19 N10 O
	883.1711	1.8	2.0	31.5	299.0	2.162	11.51	C40 H29 N9 O2 P 185Re
	883.1748	-1.9	-2.2	40.0	300.4	3.643	2.62	C49 H26 N6 185Re
	883.1708	2.1	2.4	36.0	299.1	2.323	9.80	C44 H26 N8 O2 185Re
	883.1752	-2.3	-2.6	30.0	300.9	4.108	1.64	C46 H35 O5 P 185Re
	883.1752	-2.3	-2.6	35.5	300.6	3.762	2.32	C45 H29 N7 P 185Re

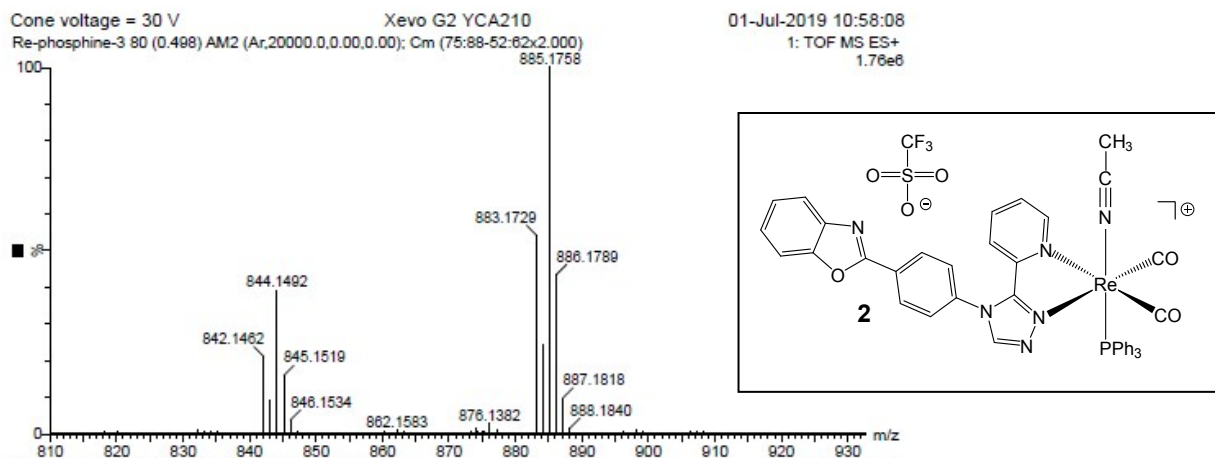


**Figure S18.** Left: High resolution mass spectrum ESI<sup>+</sup> of complex **2**, i.e. [Re(CO)<sub>2</sub>(L)(PPh<sub>3</sub>)(CH<sub>3</sub>CN)]<sup>+(OTf)</sup><sup>-</sup>, obtained by complete photolysis of complex **1-TPP** at 300 nm in acetonitrile. Only the cation is visible on the spectrum. Right: chemical structure of **2**.

### DFT and TD-DFT calculations

**Table S3.** Frontier molecular orbital compositions (%) and energy levels in CH<sub>3</sub>CN for the cation of complex **1-TPP**.

Orbital	Energy (eV)	MO Contribution (%)					Main bond type	
		Re	CO	PPh <sub>3</sub>	P <sub>1</sub>	P <sub>2</sub>		
186	LUMO+5	-1.25	3	7	75	3	12	$\pi^*(PPh_3)$
185	LUMO+4	-1.43	13	14	65	1	6	$\pi^*(PPh_3) + p(Re) + \pi^*(CO)$
184	LUMO+3	-1.57	27	35	34	3	0	$\pi^*(PPh_3) + p(Re) + \pi^*(CO)$
183	LUMO+2	-1.79	0	2	3	89	6	$\pi^*(P_1)$
182	LUMO+1	-2.23	0	0	0	4	95	$\pi^*(P_2)$
181	LUMO	-2.68	1	4	1	92	2	$\pi^*(P_1)$
HOMO-LUMO gap (E = 4.25 eV)								
180	HOMO	-6.93	0	0	0	1	99	$\pi(P_2)$
179	HOMO-1	-7.24	49	18	14	19	1	d(Re) + $\pi(CO) + \pi(P_1)$
178	HOMO-2	-7.29	50	19	24	8	0	d(Re) + $\pi(CO) + \pi(PPh_3)$
177	HOMO-3	-7.44	0	0	0	0	100	$\pi(P_2)$
176	HOMO-4	-7.46	35	15	49	0	0	$\pi(PPh_3) + d(Re) + \pi(CO)$
175	HOMO-5	-7.50	47	20	32	1	0	d(Re) + $\pi(CO) + \pi(PPh_3)$

P<sub>1</sub>: pyridyltriazole, P<sub>2</sub>: 2-phenylbenzoxazole

**Table S4.** Main electronic transitions for the cation of complex **1-TPP** in CH<sub>3</sub>CN, calculated with TD-DFT method at the PBE1PBE/LANL2DZ level, and comparison with experimental values.

Electronic transition	Contribution	Assignment	E <sub>calc</sub> /eV	λ <sub>calc</sub> /nm	f	λ <sub>exp</sub> /nm	
S <sub>0</sub> → S <sub>1</sub>	H – 1 → LUMO	d(Re) + π(CO) + π(P <sub>1</sub> ) → π*(P <sub>1</sub> )	MLCT/LLCT/ILCT	3.59	345.87	0.0175	346
S <sub>0</sub> → S <sub>2</sub>	H – 2 → LUMO	d(Re) + π(CO) + π(PPh <sub>3</sub> ) → π*(P <sub>1</sub> )	MLCT/LLCT	3.69	335.90	0.2177	
S <sub>0</sub> → S <sub>3</sub>	HOMO → LUMO	π(P <sub>2</sub> ) → π*(P <sub>1</sub> )	ILCT	3.76	329.59	0.0136	
S <sub>0</sub> → S <sub>4</sub>	H – 5 → LUMO	d(Re) + π(CO) + π(PPh <sub>3</sub> ) → π*(P <sub>1</sub> )	MLCT/LLCT	3.78	327.91	0.0054	319
S <sub>0</sub> → S <sub>5</sub>	HOMO → L + 1	π(P <sub>2</sub> ) → π*(P <sub>2</sub> )	ILCT	4.05	305.95	1.0033	305
S <sub>0</sub> → S <sub>6</sub>	H – 4 → LUMO	π(PPh <sub>3</sub> ) + d(Re) + π(CO) → π*(P <sub>1</sub> )	MLCT/LLCT	4.11	301.99	0.0086	301
S <sub>0</sub> → S <sub>7</sub>	H – 6 → LUMO	π(PPh <sub>3</sub> ) → π*(P <sub>1</sub> )	LLCT	4.23	293.43	0.0123	
S <sub>0</sub> → S <sub>11</sub>	H – 2 → L + 3	d(Re) + π(CO) + π(PPh <sub>3</sub> ) → π*(PPh <sub>3</sub> ) + p(Re) + π*(CO)	MLCT/LLCT/ILCT	4.43	280.15	0.0193	
S <sub>0</sub> → S <sub>14</sub>	H – 3 → L + 1	π(P <sub>2</sub> ) → π*(P <sub>2</sub> )	ILCT	4.48	276.76	0.0133	275
S <sub>0</sub> → S <sub>17</sub>	H – 1 → L + 2	d(Re) + π(CO) + π(P <sub>1</sub> ) → π*(P <sub>1</sub> )	MLCT/LLCT/ILCT	4.58	270.82	0.0158	268
S <sub>0</sub> → S <sub>21</sub>	H – 2 → L + 4	d(Re) + π(CO) + π(PPh <sub>3</sub> ) → π*(PPh <sub>3</sub> ) + p(Re) + π*(CO)	MLCT/LLCT/ILCT	4.73	262.16	0.0247	263
S <sub>0</sub> → S <sub>23</sub>	H – 10 → LUMO	π(PPh <sub>3</sub> ) → π*(P <sub>1</sub> )	LLCT	4.76	260.41	0.0254	
S <sub>0</sub> → S <sub>24</sub>	H – 11 → LUMO	π(P <sub>1</sub> ) → π*(P <sub>1</sub> )	ILCT	4.79	258.61	0.0546	
S <sub>0</sub> → S <sub>25</sub>	H – 12 → LUMO	π(P <sub>2</sub> ) → π*(P <sub>1</sub> )	ILCT	4.82	257.39	0.0591	
S <sub>0</sub> → S <sub>29</sub>	H – 1 → L + 4	d(Re) + π(CO) + π(P <sub>1</sub> ) → π*(PPh <sub>3</sub> ) + p(Re) + π*(CO)	MLCT/LLCT/ILCT	4.90	252.90	0.0818	
S <sub>0</sub> → S <sub>30</sub>	H – 6 → L + 1	π(PPh <sub>3</sub> ) → π*(P <sub>2</sub> )	LLCT	4.94	251.19	0.0513	

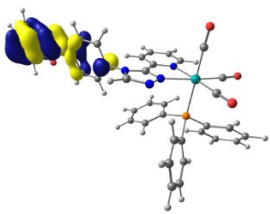
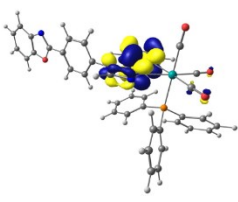
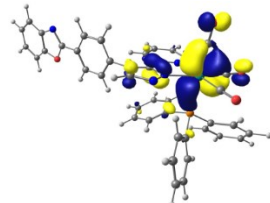
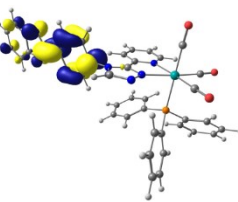
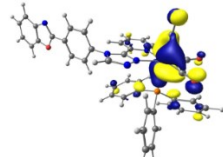
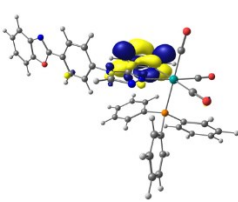
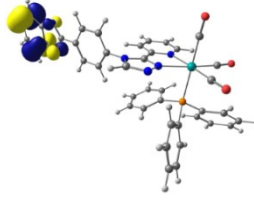
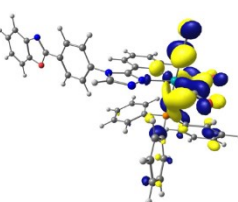
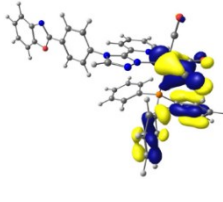
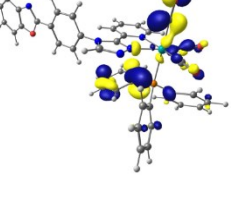
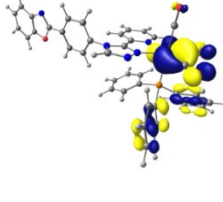
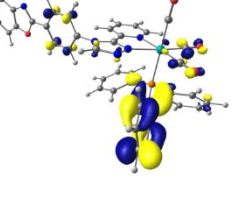
**Table S5.** Four calculated singlet states for the cation of complex **1-TPP** in S<sub>1</sub> optimized geometry with TD-DFT method at the PBE1PBE/LANL2DZ level.

State	Contribution	Assignment	E <sub>calc</sub> /eV	λ <sub>calc</sub> /nm	f
1	HOMO → LUMO	d(Re) + π(CO) + π(P <sub>1+2</sub> ) → π*(P <sub>1</sub> )	MLCT/LLCT/ILCT	2.69	460.78 0.0219
2	H – 3 → LUMO	d(Re) + π(CO) → π*(P <sub>1</sub> )	MLCT/LLCT	3.07	403.36 0.0150
3	H – 2 → LUMO	d(Re) + π(CO) + π(P <sub>1</sub> ) → π*(P <sub>1</sub> )	MLCT/LLCT/ILCT	3.14	395.50 0.4716
4	H – 1 → LUMO	π(P <sub>2</sub> ) → π*(P <sub>1</sub> )	ILCT	3.31	374.71 0.1109

**Table S6.** Calculated phosphorescence emission energies of the cation of complex **1-TPP**, in comparison to the experimental values recorded in CH<sub>3</sub>CN.

DFT			TD-DFT			λ <sub>exp</sub> (eV/nm)
ΔE <sub>T1–S<sub>0</sub></sub> (eV/nm)	Character	Major contribution (C <sub>i</sub> coefficient)	E (eV)	λ <sub>cal</sub> (nm)	Character	
2.06/601.9	<sup>3</sup> IL	L → H (0.563)	1.74	713.7	<sup>3</sup> IL π(P <sub>2</sub> ) → π*(P <sub>1+2</sub> )	544

ΔE<sub>T1–S<sub>0</sub></sub> is the energy difference between the ground singlet and triplet states.

Occupied orbitals		Unoccupied orbitals	
HOMO (-6.93 eV)		LUMO (-2.68 eV)	
HOMO-1 (-7.24 eV)		LUMO+1 (-2.23 eV)	
HOMO-2 (-7.29 eV)		LUMO+2 (-1.79 eV)	
HOMO-3 (-7.44 eV)		LUMO+3 (-1.57 eV)	
HOMO-4 (-7.46 eV)		LUMO+4 (-1.43 eV)	
HOMO-5 (-7.50 eV)		LUMO+5 (-1.25 eV)	

**Figure S19.** Isodensity plots of the frontier molecular orbitals of the cation of complex **1-TPP** in CH<sub>3</sub>CN.

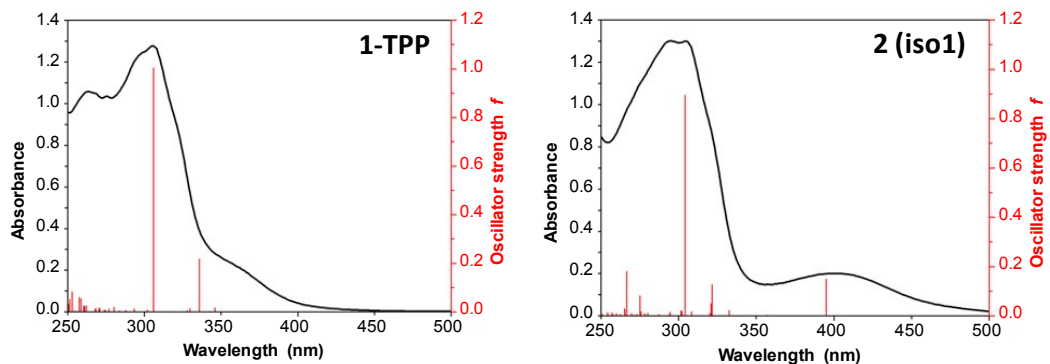


**Figure S20.** Experimental (black) and simulated (red) UV-Vis absorption spectra of complexes **1-TPP** and **2** in  $\text{CH}_3\text{CN}$ . Simulation was made for **2(iso1)**.

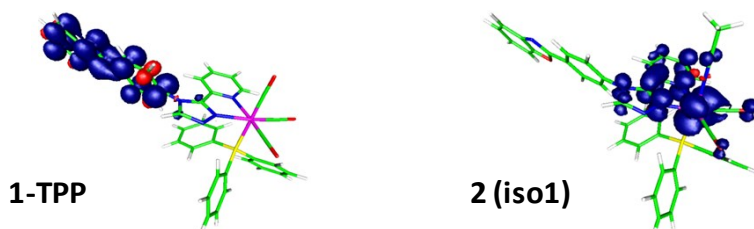


**Figure S21.** Spin density distribution for the lowest triplet state  $T_1$  of the cation of **1-TPP** and cation **2(iso1)** in  $\text{CH}_3\text{CN}$ , calculated based on the optimized triplet state with DFT method at the PBE1PBE/LANL2DZ level.

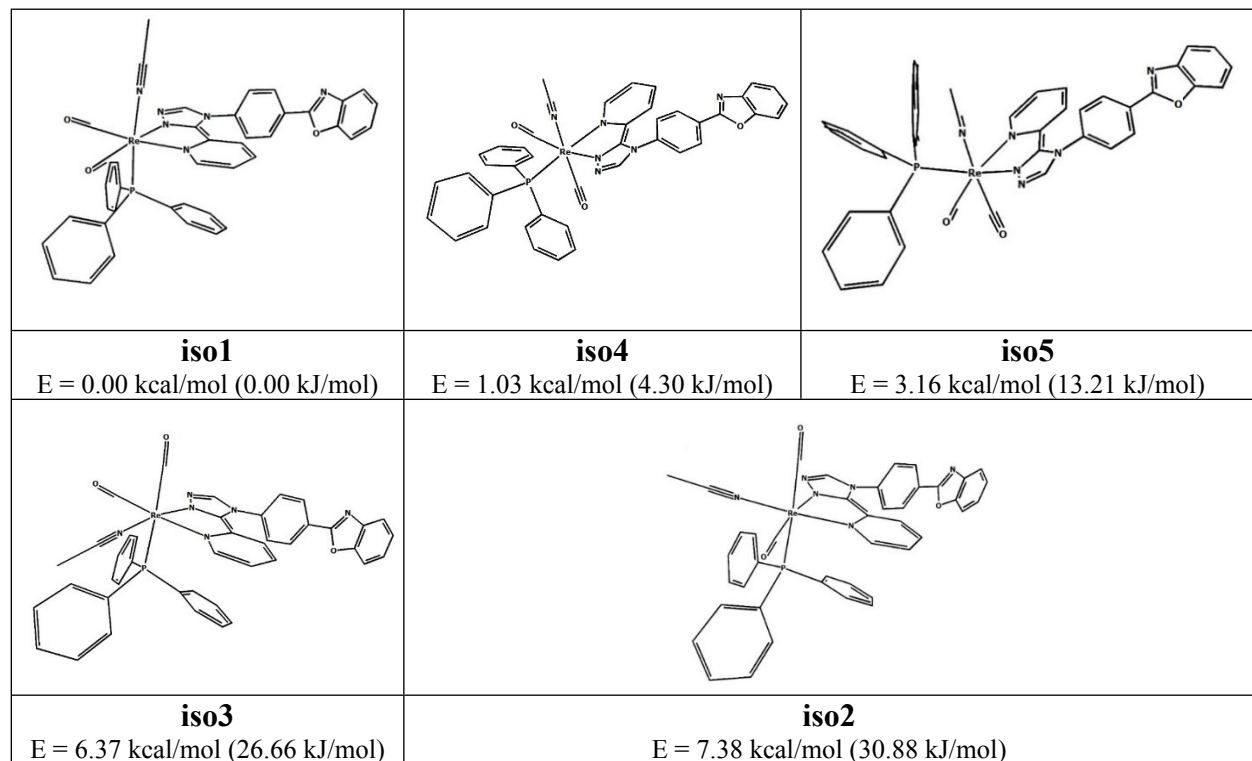


**Figure S22.** Optimized geometries of isomers 1-5 of  $[\text{Re}(\text{CO})_2(\text{L})(\text{PPh}_3)(\text{CH}_3\text{CN})]^+$  (the cation of complex **2**).

**Table S7.** Theoretical selected bond lengths [Å] and angles [°] for **2(iso1)** in CH<sub>3</sub>CN.

Bond lengths	Optimized			Bond angles	Optimized		
	S <sub>0</sub>	S <sub>1</sub>	T <sub>1</sub>		S <sub>0</sub>	S <sub>1</sub>	T <sub>1</sub>
Re(1)-C(39)	1.894	1.929	1.932	C(39)-Re(1)-C(40)	89.65	83.53	84.25
Re(1)-C(40)	1.894	1.944	1.960	C(39)-Re(1)-P(1)	90.86	90.95	91.52
Re(1)-P(1)	2.423	2.483	2.486	C(40)-Re(1)-P(1)	91.93	95.92	94.87
Re(1)-N(2)	2.169	2.104	2.073	C(39)-Re(1)-N(2)	100.46	101.52	100.31
Re(1)-N(1)	2.218	2.151	2.144	C(40)-Re(1)-N(2)	169.34	173.47	173.82
Re(1)-N(3)	2.090	2.081	2.097	P(1)-Re(1)-N(2)	91.33	88.19	89.20
				C(39)-Re(1)-N(1)	172.72	175.73	175.03
O(2)-C(39)	1.167	1.156	1.156	C(40)-Re(1)-N(1)	96.19	98.76	98.96
O(3)-C(40)	1.167	1.154	1.152	P(1)-Re(1)-N(1)	93.29	92.40	91.98
				N(2)-Re(1)-N(1)	73.48	75.94	76.22
				C(39)-Re(1)-N(3)	92.35	92.30	92.71
				C(40)-Re(1)-N(3)	92.17	91.25	89.64
				P(1)-Re(1)-N(3)	174.81	172.42	174.10
				N(2)-Re(1)-N(3)	84.08	84.46	86.00
				N(1)-Re(1)-N(3)	83.11	84.07	83.55
				O(2)-C(39)-Re(1)	178.34	177.69	177.91
				O(3)-C(40)-Re(1)	177.34	177.41	177.05

**Table S8.** Frontier molecular orbital compositions (%) and energy levels in CH<sub>3</sub>CN for cation **2(iso1)**.

Orbital	Energy (eV)	MO Contribution (%)						Main bond type	
		Re	CO	MeC N	PPh <sub>3</sub>	P <sub>1</sub>	P <sub>2</sub>		
190	LUMO+5	-1.09	2	0	1	50	5	43	$\pi^*(\text{PPh}_3) + \pi^*(\text{P}_2)$
189	LUMO+4	-1.14	4	0	1	54	4	39	$\pi^*(\text{PPh}_3) + \pi^*(\text{P}_2)$
188	LUMO+3	-1.22	4	1	2	84	1	8	$\pi^*(\text{PPh}_3)$
187	LUMO+2	-1.69	0	2	0	4	85	10	$\pi^*(\text{P}_1)$
186	LUMO+1	-2.21	0	0	0	0	7	93	$\pi^*(\text{P}_2)$
185	LUMO	-2.56	3	3	0	0	91	4	$\pi^*(\text{P}_1)$
HOMO-LUMO gap (E = 3.86 eV)									
184	HOMO	-6.42	66	16	6	5	6	0	d(Re) + $\pi(\text{CO})$
183	HOMO-1	-6.56	63	16	6	6	9	1	d(Re) + $\pi(\text{CO})$
182	HOMO-2	-6.92	0	0	0	0	1	98	$\pi(\text{P}_2)$
181	HOMO-3	-7.05	69	30	1	1	0	0	d(Re) + $\pi(\text{CO})$
180	HOMO-4	-7.34	3	1	1	95	1	0	$\pi(\text{PPh}_3)$
179	HOMO-5	-7.44	0	0	0	0	0	100	$\pi(\text{P}_2)$

P<sub>1</sub>: pyridyltriazole, P<sub>2</sub>: 2-phenylbenzoxazole

**Table S9.** Main electronic transitions for cation **2(iso1)** in CH<sub>3</sub>CN, calculated with TDDFT method at the PBE1PBE/LANL2DZ level, and comparison with experimental values.

Electronic transition	Contribution	Assignment	E <sub>calc</sub> /eV	λ <sub>calc</sub> /nm	f	λ <sub>exp</sub> /nm
S <sub>0</sub> → S <sub>1</sub>	HOMO → LUMO	d(Re) + π(CO) → π*(P <sub>1</sub> )	MLCT/LLCT	2.87	432.34	0.0008
S <sub>0</sub> → S <sub>2</sub>	H - 1 → LUMO	d(Re) + π(CO) → π*(P <sub>1</sub> )	MLCT/LLCT	3.14	394.91	0.1501
S <sub>0</sub> → S <sub>3</sub>	H - 3 → LUMO	d(Re) + π(CO) → π*(P <sub>1</sub> )	MLCT/LLCT	3.47	356.91	0.0030
S <sub>0</sub> → S <sub>4</sub>	HOMO → L + 1	d(Re) + π(CO) → π*(P <sub>2</sub> )	MLCT/LLCT	3.73	332.59	0.0220
S <sub>0</sub> → S <sub>5</sub>	H - 2 → LUMO	π(P <sub>2</sub> ) → π*(P <sub>1</sub> )	ILCT	3.86	321.50	0.1268
S <sub>0</sub> → S <sub>6</sub>	H - 1 → L + 1	d(Re) + π(CO) → π*(P <sub>2</sub> )	MLCT/LLCT	3.87	320.76	0.0502
S <sub>0</sub> → S <sub>7</sub>	HOMO → L + 2	d(Re) + π(CO) → π*(P <sub>1</sub> )	MLCT/LLCT	3.87	320.14	0.0101
S <sub>0</sub> → S <sub>8</sub>	H - 1 → L + 2	d(Re) + π(CO) → π*(P <sub>1</sub> )	MLCT/LLCT	4.02	308.40	0.0162
S <sub>0</sub> → S <sub>9</sub>	H - 2 → L + 1	π(P <sub>2</sub> ) → π*(P <sub>2</sub> )	ILCT	4.08	304.15	0.8953
S <sub>0</sub> → S <sub>10</sub>	H - 4 → LUMO	π(PPh <sub>3</sub> ) → π*(P <sub>1</sub> )	LLCT	4.10	302.22	0.0176
S <sub>0</sub> → S <sub>11</sub>	H - 4 → LUMO	π(PPh <sub>3</sub> ) → π*(P <sub>1</sub> )	LLCT	4.11	301.40	0.0211
S <sub>0</sub> → S <sub>12</sub>	H - 1 → L + 6	d(Re) + π(CO) → π*(PPh <sub>3</sub> )	MLCT/LLCT	4.21	294.54	0.0158
S <sub>0</sub> → S <sub>19</sub>	H - 3 → L + 2	d(Re) + π(CO) → π*(P <sub>1</sub> )	MLCT/LLCT	4.50	275.62	0.0169
S <sub>0</sub> → S <sub>21</sub>	H - 1 → L + 3	d(Re) + π(CO) → π*(PPh <sub>3</sub> )	MLCT/LLCT	4.51	275.00	0.0820
S <sub>0</sub> → S <sub>25</sub>	H - 11 → LUMO	π(P <sub>1</sub> ) + π(PPh <sub>3</sub> ) → π*(P <sub>1</sub> )	ILCT/LLCT	4.65	266.53	0.1802
S <sub>0</sub> → S <sub>26</sub>	H - 2 → L + 2	π(P <sub>2</sub> ) → π*(P <sub>1</sub> )	ILCT	4.67	265.36	0.0242
S <sub>0</sub> → S <sub>27</sub>	HOMO → L + 6	d(Re) + π(CO) → π*(PPh <sub>3</sub> )	MLCT/LLCT	4.68	265.19	0.0298
	HOMO → L + 7	d(Re) + π(CO) → p(Re) + π*(CO) + π*(PPh <sub>3</sub> )	MLCT/LLCT/ILCT			
S <sub>0</sub> → S <sub>35</sub>	H - 1 → L + 5	d(Re) + π(CO) → π*(PPh <sub>3</sub> ) + π*(P <sub>2</sub> )	MLCT/LLCT	4.88	254.14	0.0147
	H - 1 → L + 4	d(Re) + π(CO) → π*(PPh <sub>3</sub> ) + π*(P <sub>2</sub> )	MLCT/LLCT			

MLCT: metal-to-ligand charge transfer; LMCT: ligand-to-metal charge transfer; LLCT: ligand-to-ligand charge transfer; ILCT: intraligand charge transfer.

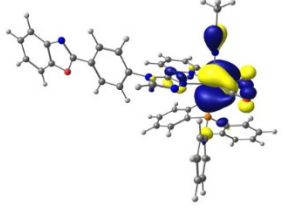
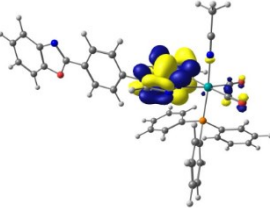
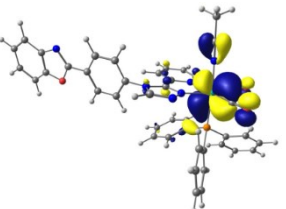
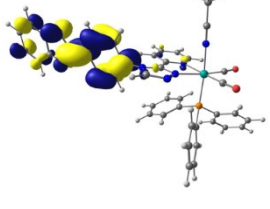
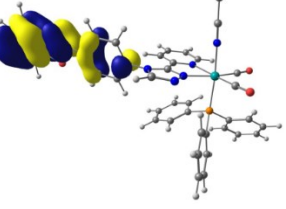
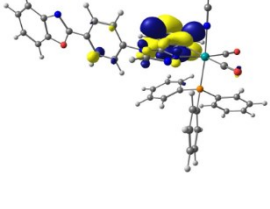
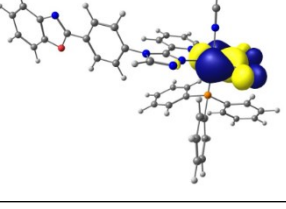
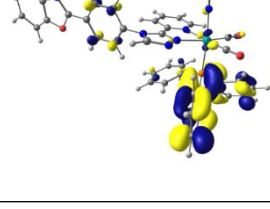
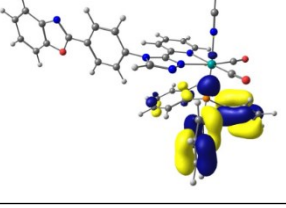
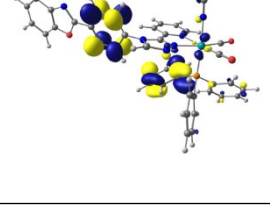
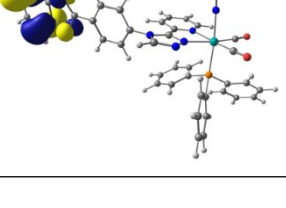
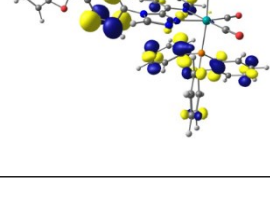
**Table S10.** Four calculated singlet states for **2(iso1)** in S<sub>1</sub> optimized geometry with TDDFT method at the PBE1PBE/LANL2DZ level.

State	Contribution	Assignment	E <sub>calc</sub> /eV	λ <sub>calc</sub> /nm	f
1	HOMO → LUMO	d(Re) + π(CO) → π*(P <sub>1</sub> )	MLCT/LLCT	2.07	599.26
2	H - 1 → LUMO	d(Re) + π(CO) → π*(P <sub>1</sub> )	MLCT/LLCT	2.65	468.29
3	H - 2 → LUMO	d(Re) + π(CO) → π*(P <sub>1</sub> )	MLCT/LLCT	2.81	441.73
4	HOMO → L + 1	d(Re) + π(CO) → π*(P <sub>2</sub> )	MLCT/LLCT	3.30	376.21

**Table S11.** Calculated phosphorescence emission energies of **2(iso1)**, in comparison to the experimental values recorded in acetonitrile.

ΔE <sub>T1-S<sub>0</sub></sub> (eV/nm)	DFT		TD-DFT			λ <sub>exp</sub> (eV/nm)
	Character	Major contribution (C <sub>i</sub> coefficient)	E (eV)	λ <sub>cal</sub> (nm)	Character	
1.74/712.6	<sup>3</sup> MLCT/ <sup>3</sup> LLCT/ <sup>3</sup> IL	L → H (0.679)	1.75	707.6	<sup>3</sup> MLCT/ <sup>3</sup> LLCT d(Re)+π(CO) → π*(P <sub>1</sub> )	686

ΔE<sub>T1-S<sub>0</sub></sub> is the energy difference between the ground singlet and triplet states.

Occupied orbitals		Unoccupied orbitals	
HOMO (-6.42 eV)		LUMO (-2.56 eV)	
HOMO-1 (-6.56 eV)		LUMO+1 (-2.21 eV)	
HOMO-2 (-6.92 eV)		LUMO+2 (-1.69 eV)	
HOMO-3 (-7.05 eV)		LUMO+3 (-1.22 eV)	
HOMO-4 (-7.34 eV)		LUMO+4 (-1.14 eV)	
HOMO-5 (-7.44 eV)		LUMO+5 (-1.09 eV)	

**Figure S23.** Isodensity plots of the frontier molecular orbitals of cation **2(iso1)** in CH<sub>3</sub>CN.

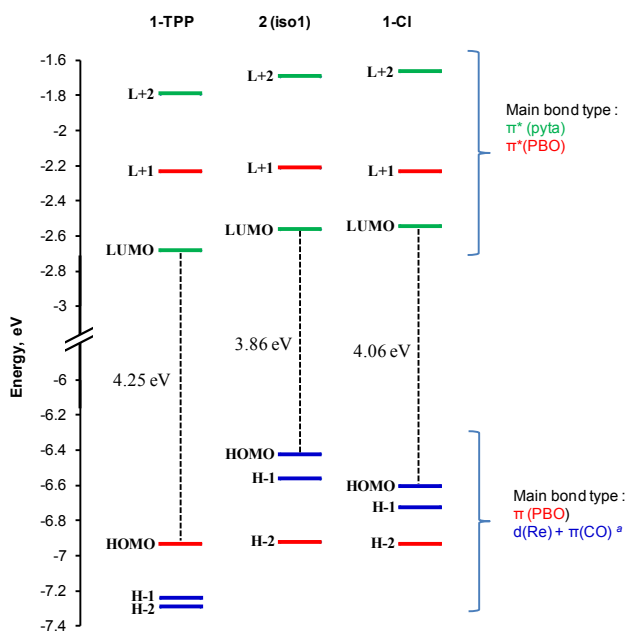


**Figure S24.** Comparative energy levels of selected frontier molecular orbitals of the cation of complex 1-TPP, cation 2(iso1) in  $\text{CH}_3\text{CN}$ , and complex 1-Cl in  $\text{CH}_2\text{Cl}_2$  (Wang et al, *Dalton Trans.*, 2019, **48**, 15906–15916) according to TD-DFT calculations at the PBE1PBE/LANL2DZ level of theory.